Open Research Online

Citation

Bowen, James; Cheneler, David; Walliman, Dominic; Arkless, Stuart G; Zhang, Zhibing; Ward, Michael C. L. and Adams, Michael J. (2010). On the calibration of rectangular atomic force microscope cantilevers modified by particle attachment and lamination. Measurement Science and Technology, 21(11), article no. 115106.

URL

https://oro.open.ac.uk/43189/

License

(CC-BY-NC-ND 4.0)Creative Commons: Attribution-Noncommercial-No Derivative Works 4.0

Policy

This document has been downloaded from Open Research Online, The Open University's repository of research publications. This version is being made available in accordance with Open Research Online policies available from Open Research Online (ORO) Policies

Versions

If this document is identified as the Author Accepted Manuscript it is the version after peer review but before type setting, copy editing or publisher branding

On the calibration of rectangular atomic force microscopy cantilevers modified by particle attachment and lamination

James Bowen, [†] *David Cheneler,* [⊥] *Dominic Walliman,* [‡] *Stuart G. Arkless,* [▲] *Zhibing Zhang,* [†] *Michael C.L. Ward* [⊥] *Michael J. Adams,* [†,*]

[†] School of Chemical Engineering, The University of Birmingham, Edgbaston, Birmingham, B15 2TT, UK

[⊥] School of Mechanical Engineering, The University of Birmingham, Edgbaston, Birmingham, B15 2TT, UK

[‡] School of Physics and Astronomy, The University of Birmingham, Edgbaston, Birmingham, B15 2TT, UK

[▲] School of Chemistry, The University of Birmingham, Edgbaston, Birmingham, B15 2TT, UK

* To whom correspondence should be addressed

Email: m.j.adams@bham.ac.uk
Telephone: + 44 (0) 121 414 5297
Fax: +44 (0) 121 414 5377

Abstract

A simple but effective method for estimating the spring constant of commercially available atomic force microscopy (AFM) cantilevers is presented, based on estimating the cantilever thickness from knowledge of its length, width, resonant frequency and the presence or absence of an added mass, such as a colloid probe at the cantilever apex, or a thin film of deposited material. The spring constant of the cantilever can then be estimated using standard equations for cantilever beams. The results are compared to spring constant calibration measurements performed using reference cantilevers. Additionally, the effect of the deposition of Cr and Ti thin films onto rectangular Si cantilevers is investigated.

Keywords

atomic force microscopy, cantilever, calibration, spring constant, resonant frequency, thin film, vacuum evaporation, gold, chromium, titanium, X-ray photoelectron spectroscopy

1. Introduction

The calibration of the spring constants of atomic force microscopy (AFM) cantilevers has been an issue of interest to researchers since Hutter and Bechhoefer [1] and Sader *et al*. [2] published the original, and now highly-cited, studies in the 1990s. Indeed, it is a topic which continues to be of interest, with ever-increasing numbers of AFM users and research areas applying the technique to study topographies and force interactions on a increasingly extensive variety of materials. Spring constant calibration has been investigated using various experimental and theoretical methods but there is still no real consensus on what is the most appropriate available method. In 2005, Clifford and Seah published a comprehensive review and comparison of many of the methods available [3], which encompassed dimensional, static and dynamic experimental techniques. As the AFM industry progresses, a wide variety of commercially available modified cantilevers can now be purchased from specialised suppliers, providing researchers with unprecedented access to custom cantilever tips, cantilevers with attached colloid probes and cantilevers laminated with metals such as Al, Ti, Cr and Au. To the best of our knowledge, the application of spring constant calibration methods to these modified cantilevers has not previously been dealt with, and the modifications of the beams do not necessarily lend themselves to simple analysis. Experimental calibration methods affording spring constant determination often require that the original beam properties are modified slightly, perhaps by the addition of a point mass [4] or a thin film of vacuum deposited metal [5]. The use of microelectromechanical systems actuators [6], piezosensors [7] and reference springs [8] and nanoindenters [9] have all been proposed. Additionally, efforts have been made to better understand the mechanics of AFM cantilevers through the use of geometrical modelling [10], and also through examining the distribution of spring constants for cantilevers fabricated from the same wafer [11]. Many of these methods of calibration offer accuracy, but are time-consuming and often require instrumentation not available to all AFM researchers.

The objective of this paper is to provide a quick and simple methodology in order that AFM experimentalists can, to a reasonable degree, estimate rectangular cantilever spring constants using only measurements of the cantilever width, length and resonant frequency, rather than go through a systematic calibration procedure. Such measurements would not require modification of the cantilevers in any way prior to their intended use. The analysis does not extend to laminated triangular or V-shaped cantilevers, which are often employed in AFM experiments. Such cantilevers pose a much greater mechanical problem and significant previous research has focussed on the calibration of such beams [3].

It is hoped that the equations and methods demonstrated in this paper will be of real value and usefulness to AFM researchers as quick and simple first order approximations of estimating cantilever spring constants, which can then be followed-up with more detailed calibrations if required. The cantilever thickness is first calculated, followed by the cantilever spring constant, which is then compared with the spring constant measured using the method of Tortonese and Kirk [12], whereby microfabricated reference cantilevers are employed as calibration standards.

2. Theory

Given that the length, width and resonant frequency of AFM cantilevers can be reasonably measured using the optical microscope system incorporated into most modern AFMs, it is assumed that these parameters are measurable or available for any type of cantilever for which the spring constant is estimated using the method presented here. Additionally, the properties of the cantilever material, which is typically Si or Si_3N_4, are assumed to be the same as the bulk literature properties for the material.

2.1 Rectangular beams and rectangular beam with an added mass

As stated initially by Cleveland *et al.* [4] for the purposes of spring constant calibration, it is well-established that for a rectangular beam, the spring constant, k, is given by Equation (1):

$$k = \frac{E_b w t^3}{4L^3} \qquad (1)$$

where, E_b is the Young's modulus of the beam material, w is the width of the beam, t is the thickness of the beam and L is the length of the beam.

The resonant frequency, v, of a rectangular beam is related to the spring constant and beam mass by Equation (2):

$$v = \frac{1}{2\pi}\left(\frac{k}{m_0^*}\right)^{0.5} \qquad (2)$$

where, $m_0^* = 0.24 M_b = 0.24 \rho_b L w t$, in which m_0^* is the effective mass of the beam, M_b is the mass of the beam, and ρ_b is the density of the beam material.

Combining Equations (1) and (2) and rearranging for the cantilever thickness yields:

$$t = \left(\frac{3.84 L^4 \rho_b \pi^2 \nu^2}{E_b} \right)^{0.5} \qquad (3)$$

Equation (3) can be used to calculate the thickness of a rectangular cantilever, provided that the length, width, resonant frequency and material properties of the cantilever are known.

For a commercially available cantilever with an added mass, M_{add}, at its apex, such as a colloid particle, $m_0^* = 0.24 \rho_b L w t + M_{add}$, and in this case combining Equations (1) and (2) yields:

$$\nu = \frac{1}{2\pi} \left(\frac{E_b w t^3}{4L^3} \right)^{0.5} \left(\frac{1}{0.24 \rho_b L w t + M_{add}} \right)^{0.5} \qquad (4)$$

Equation (4) can be rearranged to give a third-order polynomial for t:

$$E_b w t^3 - 3.84 \rho_b L^4 w \pi^2 \nu^2 t - 16 \pi^2 \nu^2 L^3 M_{add} = 0 \qquad (5)$$

Equation (5) can then be solved either graphically or by using Cardano's solution [13] if a valid solution can be found given the limits of that particular method.

When there is an added mass present at the apex of a beam, it has previously been shown [2] that the spring constant should be adjusted for the positioning of the added mass using Equation (6):

$$k_{adjusted} = k_{unadjusted} \left(\frac{L}{L-d} \right)^3 \qquad (6)$$

where, d is the distance from the beam apex to the centre of the added mass. For a beam with no added mass, d equals zero.

Combining Equations (2) and (6) then yields an expression for the beam spring constant:

$$k = 4\pi^2 \nu^2 \left(0.24\rho_b Lwt + M_{add}\right)\left(\frac{L}{L-d}\right)^3 \tag{7}$$

It should be noted that the equations presented here could also be used to calculate the mass added onto a cantilever:

$$M_{add} = \frac{E_b wt^3}{16\pi^2 \nu^2 L^3} - 0.24\rho_b Lwt \tag{8}$$

where, t can be calculated using Equation (3).

2.2 Laminated rectangular beams

For a rectangular beam laminated with a uniform layer across the upper and lower surfaces of the beam, an effective flexural modulus, E_b, can be calculated according to the number of laminating layers using the expression [14]:

$$E_b = \frac{8}{t_b^3}\sum_{j=1}^{N/2}(E)_j\left(z_j^3 - z_{j-1}^3\right) \tag{9}$$

where, t_b is the beam thickness, j indicates the layer of interest, E_j is the Young's modulus of layer j and z_j is the thickness of layer j.

For the cantilever beams considered here, both the upper and lower surfaces of the Si beam are coated with layers of Cr and a layer of Au. The layer of Cr is the same thickness on both the upper and lower surfaces, as is the layer of Au. In this case, Equation (9) becomes:

$$E_b = \frac{8}{t_b^3}\left\{E_{Si}\left(\frac{t_{Si}}{2}\right)^3 + E_{Cr}\left[\left(\frac{t_{Si}}{2}+\frac{t_{Cr}}{2}\right)^3 - \left(\frac{t_{Si}}{2}\right)^3\right] + E_{Au}\left[\left(\frac{t_b}{2}\right)^3 - \left(\frac{t_{Si}}{2}+\frac{t_{Cr}}{2}\right)^3\right]\right\} \tag{10}$$

where, t_{Si} is the thickness of the Si beam, t_{Cr} and t_{Au} are the total thicknesses of the Cr and Au layers deposited respectively, and E_{Si}, E_{Cr} and E_{Au} are the Young's moduli of the Si beam, the Cr layer and the Au layer respectively. The thickness of laminating layers can be monitored *in situ* using a quartz crystal microbalance (QCM) during the deposition process. For commercially available cantilevers, the thickness of the laminating layers should be available from the supplier. Independent assessment of the thickness of laminating layers can be performed using ellipsometry, for example.

As the beam is laminated uniformly across its width and length, the expression for the effective density of the beam, ρ_b, can be formulated simply, based on the relative thicknesses of the three materials:

$$\rho_b = \frac{t_{Si}}{t_b}\rho_{Si} + \frac{t_{Cr}}{t_b}\rho_{Cr} + \frac{t_{Au}}{t_b}\rho_{Au} \qquad (11)$$

When Equations (10) and (11) are substituted into Equations (1) and (2), it is not trivial to obtain an expression for t comparable to Equation (3). However, as a first order approximation, Equations (10) and (11) can be substituted into Equation (5), which can then be solved graphically.

3. Experimental details

3.1 Spring constant comparison with theory

The spring constants of three different types of commercially available cantilevers were investigated: rectangular Si cantilevers (MikroMasch, USA), rectangular Si cantilevers with attached SiO_2 microparticles (NovaScan, USA), and rectangular Si cantilevers laminated with 20 nm thickness Cr and 20 nm thickness Au thin films on both sides (MikroMasch, USA). The resonant frequencies of the cantilevers investigated were measured using a NanoWizard II AFM (JPK, UK. The base of each cantilever was oscillated sinusoidally over a suitable frequency range and the resultant amplitude of deflection of the cantilever was monitored as a function of frequency. The resonant frequencies of the cantilevers investigated here are listed in Tables 1-3. The spring constants of the cantilevers were measured by the method described by Tortonese and Kirk [12], using rectangular Si reference cantilevers (Veeco, USA). Briefly, the method consists of comparing the deflection of the cantilever of interest when pressed against a hard reference surface, such as a Si wafer, with the deflection when pressed against a reference cantilever of known spring constant. The difference between the two deflection gradients is directly proportional to the spring constant of the cantilever to be calibrated and can be simply calculated.

3.2 Investigation of the lamination of Si surfaces

The process of laminating a Si beam with a metal such as Ti or Cr was investigated by depositing atomic Ti or Cr onto rectangular Si cantilevers and monitoring the effect on the measured resonant frequency of the beam. Simultaneously, Ti or Cr was deposited onto a Si wafer and the thickness, surface structure and

chemical composition of the deposited layer could be assessed, using ellipsometry, atomic force microscopy and X-ray photoelectron spectroscopy respectively. The objective of this investigation was to explore the possibility of surface stress being induced on the cantilever beam. In addition, the interaction between Ti and Au, and the interaction between Cr and Au, was also investigated using the above techniques.

3.2.1 Vacuum deposition of metals

Ti and Cr (Kurt J. Lesker, USA) thin films were deposited by electron beam evaporation onto rectangular Si cantilevers (MikroMasch, USA) and Si wafers (IDB Technologies, UK) using an Auto 500 evaporation system (Edwards, UK). Films were deposited at a rate of 0.01-0.1 nm/s and film thicknesses were monitored *in situ* using a QCM (Edwards, UK).

3.2.2 Ellipsometry

Ellipsometry measurements were performed using a spectroscopic ellipsometer (Jobin-Yvon/Horiba, UK) operating with DeltaPsi2 v2.0.8 software. The angle of incidence was set to 70°. The wavelength range for the incident light was 250-800 nm. All measurements were made under conditions of ambient temperature, pressure and humidity. Precautions were taken to avoid performing measurements on visibly defective sample locations. Calculation of metal film thicknesses was performed for each measurement, based on a three-phase ambient/thin film/Si model, in which the thin film was assumed to be isotropic and modelled using a simple classical layer model, whose initial thickness was varied using a multiguess iterative calculation procedure.

3.2.3 Atomic force microscopy

AFM images of the metal films were acquired using a MultiMode AFM (Veeco, UK) housed on a vibration isolation table. Nanoscope v5.12 software (Veeco, UK) was used for both real-time analysis and post-capture image processing. All images were acquired while operating in Tapping Mode under ambient conditions, using a rectangular 180 µm length pyramidal-tipped Si cantilever (RTESP, Veeco, UK) with a nominal spring constant of 40 N m^{-1}, a nominal resonant frequency of 300 kHz, and a nominal tip diameter of 20 nm. All images were acquired at scan rates between 0.5-1.0 Hz with each image being composed of 512 x 512 pixels. All images were subsequently analysed for the root-mean-square roughness (R_q), average roughness (R_a) and z-range of the deposited thin film surfaces. The purpose of measuring film surface roughness was to ensure that the deposited film was of sufficiently low roughness so that it could be treated as a continuous layer. The resonant frequencies of Si cantilevers onto which Ti or Cr was deposited were measured as described in Section 3.1.

3.2.4 X-ray photoelectron spectroscopy

XPS analysis of thin films was performed using a custom-built instrument operating an Al κα X-ray source, providing a monochromatic X-ray beam with incident energy of 1486.68 eV. The measurements were made at a pressure of ~ 1 x 10^{-8} mbar and with a circular spot size of ~ 4 mm^2. Samples were immobilised onto stainless steel sample holders using double-sided carbon sticky tape (Shintron tape, Agar Scientific, UK). Low resolution survey spectra were obtained using a pass energy of 150 eV over a binding energy range of -10 to 1,200 eV with 1 eV increments. High resolution spectra were obtained using a pass energy of 20 eV

over a binding energy range of 20-30 eV, centred around a chosen photoelectron binding energy with 0.1 eV increments. A dwell time of 500 ms was employed when collecting data from each binding energy increment for all measurements.

4. Results and discussion

4.1 Comparison of measurement and calculation

The calculated thicknesses and spring constants of the cantilevers investigated are listed in Tables 1-3, alongside their measured spring constants. Figures 1-3 illustrate the correlation between the measured spring constants and the calculated spring constants, the percentage deviation between measured and calculated spring constants, and the relationship between resonant frequency and spring constant for the three types of cantilever investigated. The results show that there is reasonable agreement between the measured and calculated spring constants for both the rectangular cantilevers (R01-R09) and the rectangular cantilevers with 12 μm diameter SiO_2 microparticles attached at their apex (P01-P09), with a slight tendency for the calculation method to overestimate when compared with the measured spring constant. However, for the rectangular cantilevers laminated with Cr and Au thin films, there is a systematic underestimation of the spring constant when compared with the measured value. The measured spring constant is typically twice the calculated spring constant. Following the method employed by Sader *et al.* [2] for dealing with thin films deposited onto cantilevers, the resonant frequencies of the unlaminated cantilevers can be estimated using Equation (12):

$$\nu_{unlaminated} = \nu_{laminated}\left\{1+\left[\left(\frac{t_{Cr}}{t_{Cr}+t_{Au}}\right)\frac{(\rho_{Cr}+\rho_{Au})}{\rho_{Si}}\right]\left[\frac{t_{Cr}+t_{Au}}{t_{Si}}\right]\right\}^{0.5} \quad (12)$$

The modified resonant frequency can be used to calculate the unlaminated cantilever thickness and spring constant, and these results are also shown in Table 3. However, it is apparent that even when the resonant frequency is adjusted using Equation (12), the spring constants are still underestimated for the laminated cantilevers.

When thermally evaporated or sputter deposited, Au thin films do not adhere particularly well to Si/SiO_2 surfaces, and therefore a Cr or Ti thin film is often used as an adhesion promoter [15]. The Si cantilever has a native SiO_2 layer of thickness 1-3 nm present at the ambient interface, the SiO_2 layer having a tetrahedral structure [16]. When Cr and Ti are thermally evaporated onto the beam, the nature of the interaction with and adhesion of the metal to the SiO_2 surface could lead to the formation of partially oxidised layers due to the reaction of the atomic metal with the surface oxygen atoms of the SiO_2, leading to a structural mismatch between the SiO_2 and the metal adhesive layer. For example, Cr_2O_3 has a hexagonal close packed structure [17-18] and does not match well with the tetrahedral structure of the SiO_2. The structure of the TiO_2 layer formed from deposited Ti could be more complicated, as TiO_2 has three allotropic forms, all with different crystal structures [19]. However, none of these structures match perfectly with the SiO_2 found at the cantilever outer surface. It is hypothesised that the mismatch between the structures of the SiO_2 and the metal oxide may confer additional stress to the beam surface. The effect of such an additional stress could lead to a beam that is significantly more difficult to deflect than it would otherwise have been, and therefore has a higher spring constant, than can be predicted using currently available theories.

The calculated and measured values for the spring constant for the laminated beams are given in Table 3. Modelling the additional surface stress as a simple axial load, using the exact expression for the stiffness of a cantilever with simultaneous axial and transverse loading, [20] we obtain the relationship:

$$k = \frac{T}{L - \sqrt{\frac{EI}{T}} \tan\left(L / \sqrt{\frac{EI}{T}}\right)} \tag{13}$$

where, I is the area moment of inertia and is given by [21]:

$$I = \frac{w t_b^{\,3}}{12} \tag{14}$$

For cantilevers L01-L09, the mean additional load required to be induced by the deposition of the metal films, so that the calculated and measured spring constants are equivalent, is 3.5 ± 1.0 mN. This result is quite consistent for shorter beams, and fluctuates more for longer beams. However, for the commercially available laminated cantilevers investigated here, as a good approximation, the measured spring constants were generally found to be twice the value of the calculated spring constant, and therefore the calculated values could be multiplied by two in order to provide an order-of-magnitude estimate of the actual spring constant of these laminated beams.

In an attempt to gain further understanding of the effect of laminating Si cantilevers with metals that form stable oxides, a series of rectangular Si cantilevers were coated with thin films of Cr or Ti, and the change in resonant frequency was monitored. Ellipsometry was used to verify the thickness of the deposited metal film. The r_a and r_{RMS} roughness of the metal films, as measured by AFM, was less 1 nm for both Cr and Ti. Table 4 shows the change in resonant frequencies, and reveals that the resonant frequency of the beams increased slightly, a surprising result given that the addition of mass to the cantilever should have served to decrease the resonant frequency of the beam, which suggests that metal deposition confers stress upon the upper surface of the beam. XPS analysis of the cantilevers yielded surface compositions as shown in Table 5, noting that Ti was present exclusively in the form of TiO_2 (binding energy 457.5 eV), whereas Cr was present as both Cr (binding energy 573 eV) and Cr_2O_3 (binding energy 575.5 eV).

4.2 Effect of uncertainty

The uncertainties involved for the different system parameters will have an effect on the calculated thickness and spring constant, and it is useful to attempt to quantify these for a typical system. Table 6 lists typical uncertainties associated with the cantilever length, width, resonant frequency, Young's modulus and material

density. For a rectangular Si cantilever of nominal dimensions l = 90 µm, w = 35 µm, with ν = 344.431 kHz, ρ_b = 2,330 kg/m^3 and E_b = 152 GPa [3], the thickness and spring constant are calculated to be 2.13 µm and 17.54 N/m respectively. Table 6 shows the deviation in t and k calculated according to the magnitude of each uncertainty, and as can be seen, l and w have the most appreciable impact on the estimation of cantilever spring constant. However, given the ease of measurement of l, w and ν for rectangular cantilevers, and the short amount of time required to calculate the spring constant following these measurements, an error of 0.5-0.6 N/m for a cantilever with a spring constant of 17.54 N/m could be considered acceptable. The optical microscope integrated with the AFM was calibrated using a Si graticule (Agar Scientific, UK) showing an array of squares with periodicity 10 µm. When a high level of magnification was chosen using the optical microscope zoom system (Navitar, USA), an uncertainty of ±1 µm was found in determining lateral dimensions. Hence, an uncertainty of ±1 µm was incorporated when measuring l and w. Going on to quantify the effect of uncertainty propagation for the same cantilever, if the upper and lower bounds for the uncertainties on each of l, w, ν, ρ_b and E_b were used in order to estimate the cantilever spring constant, according to Equations (1) and (3), the resultant error would be 2.3 N/m, which is equivalent to 13 % of the calculated spring constant. These calculations are shown in Table 7. This error may be of an acceptable magnitude to those experimentalists who simply require a quick and simple estimate of cantilever spring constant. Indeed, the uncertainty is comparable to the uncertainties associated with experimental methods such as thermal noise analysis, dynamic mass attachment and static mass hanging [3]. However, this method requires less time and resources on the part of the experimentalist, and can also be applied to modified rectangular beams.

4.3 Effect of beam clamping

It should be noted that although the cantilever is a clamped free beam, the clamp which holds it is not perfectly stiff. Compression of a spring clip for the NanoWizard II AFM, using a Z030 mechanical tester (Zwick/Roell, UK) revealed that the spring clip has a spring constant on the order of 5,000 N/m, which is two orders of magnitude greater than the stiffest typical AFM cantilever. Therefore, although the clamp which holds the cantilever is not perfectly stiff, it has a stiffness much greater than the AFM cantilever it is used to hold. The effect of increasing the drive amplitude of the cantilever base on the measured amplitude and resonant frequency of a number of cantilevers was subsequently investigated. The cantilevers tested were (i) rectangular CSC12 and NSC12 series (Mikro Masch, Estonia), (ii) rectangular CSC12 and NSC12 series laminated with Cr and Au (Mikro Masch, Estonia), and (iii) rectangular with 6 μm radius SiO_2 colloid probe attached at the apex (Novascan, USA). With the exception of the laminated NSC12 cantilevers, there was no change in resonant frequency with increasing drive amplitude, and the measured cantilever amplitude at resonance scaled linearly with the drive amplitude. Interestingly, there was a slight increase in resonance frequency with increasing drive amplitude for the laminated NSC12 cantilevers, with an increase of 19 Hz exhibited as the amplitude at resonance was increased from 10.3 nm to 41.8 nm. The NSC12 cantilevers are the heaviest beams investigated, and therefore there is a possibility that as the mass of the resonating beam increases, the potential for the spring which clamps the cantilever in place to affect the measured resonant frequency also increases. However, the effect observed for the NSC12 cantilevers was small (0.19 kHz increase from an initial resonant frequency of 205.372 kHz) and was not observed for any other type of cantilever.

5. Conclusions

A simple method for calculating the spring constant of different types of commercially available AFM cantilevers, based on the length, width, resonant frequency and the presence or absence of an added mass or laminating layer, has been presented and compared with spring constant measurements using reference cantilevers. The estimation of spring constants for rectangular cantilevers and rectangular cantilevers with added masses, such as microparticles attached to their apex, was found to be in reasonable agreement with the measured values. In contrast, the method tended to underestimate the spring constants of laminated rectangular beams, which may be an effect of the nature of the adhesion of Cr to the SiO_2 surface of the Si beam. The lamination of Si cantilevers with thin films of metal that form oxides appears to induce additional stresses at the cantilever surface, which influences the measured resonant frequency and spring constant in a complex fashion, which is currently the subject of further investigation. Additionally, the resonant frequency of the majority of AFM cantilevers investigated was found not to be a function of the amplitude at which it was oscillated, even though the beam is clamped into place in an AFM with a spring of finite stiffness.

Acknowledgements

The AFM used in this research was obtained through Birmingham Science City: Innovative Uses for Advanced Materials in the Modern World (West Midlands Centre for Advanced Materials Project 2), with support from Advantage West Midlands (AWM) and part funded by the European Regional Development Fund (ERDF). The University of Birmingham and Unilever Research & Development are acknowledged for financial support for JB and DC. Dr Parvez Iqbal, Dr Christopher Hamlett, Simon Leigh and Nazia Mehrban at the University of Birmingham are all thanked for useful discussions.

References

1. Hutter, J.L., Bechhoefer, J., Calibration of atomic force microscope tips, *Rev. Sci. Instrum.*, **1993**, *64 (7)*, 1868-1873.
2. Sader, J.E., Larson, I., Mulvaney, P., White, L.R., Method for the calibration of atomic force microscope cantilevers, *Rev. Sci. Instrum.*, **1995**, *66 (7)*, 3789-3798.
3. Clifford, C.A., Seah, M.P., The determination of atomic force microscope cantilever spring constants via dimensional methods for nanomechanical analysis, *Nanotechnology*, **2005**, *16*, 1666-1680.
4. Cleveland, J.P., Manne, S., Bocek, D., Hansma, P.K., A nondestructive method for determining the spring constant of cantilevers for scanning force microscopy, *Rev. Sci. Instrum.*, **1993**, *64 (2)*, 403-405.
5. Gibson, C.T., Weeks, B.L., Lee, J.R.I., Abell, C., Rayment, T., A nondestructive technique for determining the spring constant of atomic force microscope cantilevers, *Rev. Sci. Instrum.*, **2001**, *72 (5)*, 2340-2343.
6. Gao, S., Zhang, Z., Wu, Y., Herrmann, K., Towards quantitative determination of the spring constant of a scanning force microscope cantilever with a microelectromechanical nano-force actuator, *Meas. Sci. Technol.*, **2010**, *21*, 015103.
7. Langlois, E.D., Shaw, G.A., Kramar, J.A., Pratt, J.R., Hurley, D.C., Spring constant calibration of atomic force microscopy cantilevers with a piezosensor transfer standard, *Rev. Sci. Instrum.*, **2007**, *78*, 093705.
8. Cumpson, P.J., Zhdan, P., Hedley, J., Calibration of AFM cantilever stiffness: a microfabricated array of reflective springs, *Ultramicroscopy*, **2004**, *100*, 241-251.
9. Clifford, C.A., Seah, M.P., Improved methods and uncertainty analysis in the calibration of the spring constant of an atomic force microscope cantilever using static experimental methods, *Meas. Sci. Technol.*, **2009**, *20*, 125501.
10. Marinello, F., Bariani, Carmignato, S., Savio, E., Geometrical modelling of scanning probe microscopes and characterization of errors, *Meas. Sci. Technol.*, **2009**, *20*, 084013.

11. Webber, G.B., Stevens, G.W., Grieser, F., Dagastine, R.R., Chan, D.Y.C., Variations in properties of atomic force microscope cantilevers fashioned from the same wafer, *Nanotechnology*, **2008**, *19*, 105709.
12. Tortonese, M., Kirk, M., Characterization of application specific probes for SPMs, *Micromachining and Imaging*, **1997**, *3009*, 53-60.
13. James, G., Modern Engineering Mathematics 2nd Edition, *Addison-Wesley (Harlow)*, **1996**, p169.
14. Gibson, R.F., Principles of Composite Material Mechanics, *McGraw-Hill (New York; London)*, **1994**, p194.
15. Schneider, M., Mohwald, H., Akari, S., Quantitative measurement of chromium's ability to promote adhesion, *J. Adhesion*, **2003**, *79*, 597-607.
16. Iler, R.K., The Colloid Chemistry of Silica and Silicates, *Cornell University Press (New York)*, **1955**, p234.
17. Jiang, N., Silcox, J., Observations of reaction zones at chromium-oxide glass interfaces, *J. Appl. Phys.*, **2000**, *87 (8)*, 3768-3776.
18. Reddy, B.V., Khanna, S.N., Ashman, C., Oscillatory magnetic coupling in Cr_2O_n (n=1-6) clusters, *Phys. Rev. B*, **2000**, *61 (8)*, 5797-5801.
19. Douglas, B.E., Ho, S-M., Structure and Chemistry of Crystalline Solids, *Springer (New York)*, **2006**, p78.
20. Young, W.C., Budynas, R.G., Roark's Formulas for Stress and Strain, 4th Edition, *McGraw-Hill (UK)*, **1965**, p148.
21. Pytel, A., Kiusalaas, J., Engineering Mechanics: Statics, 2nd Edition, *Brooks/Cole (USA)*, **1999**, p424.

Figure captions

Figure 1. Correlation between measured spring constants and calculated spring constants for all types of cantilever

Figure 2. Percentage deviation between measured and calculated spring constants

Figure 3. Measured spring constants as a function of cantilever resonant frequency

Table captions

Table 1. Measured and calculated properties of rectangular cantilevers

Table 2. Measured and calculated properties of rectangular cantilevers modified with SiO_2 microparticles

Table 3. Measured and calculated properties of rectangular cantilevers laminated with 20 nm Cr and 20 nm Au thin films

Table 4. Change in resonant frequencies of rectangular Si cantilevers upon deposition of thin films of Cr or Ti

Table 5. Percentage compositions of cantilever surfaces after deposition of thin films of Cr or Ti

Table 6. Uncertainties associated with system parameters

Table 7. Effect of uncertainty propagation

Figures

Figure 1. Correlation between measured spring constants and calculated spring constants for all types of cantilever

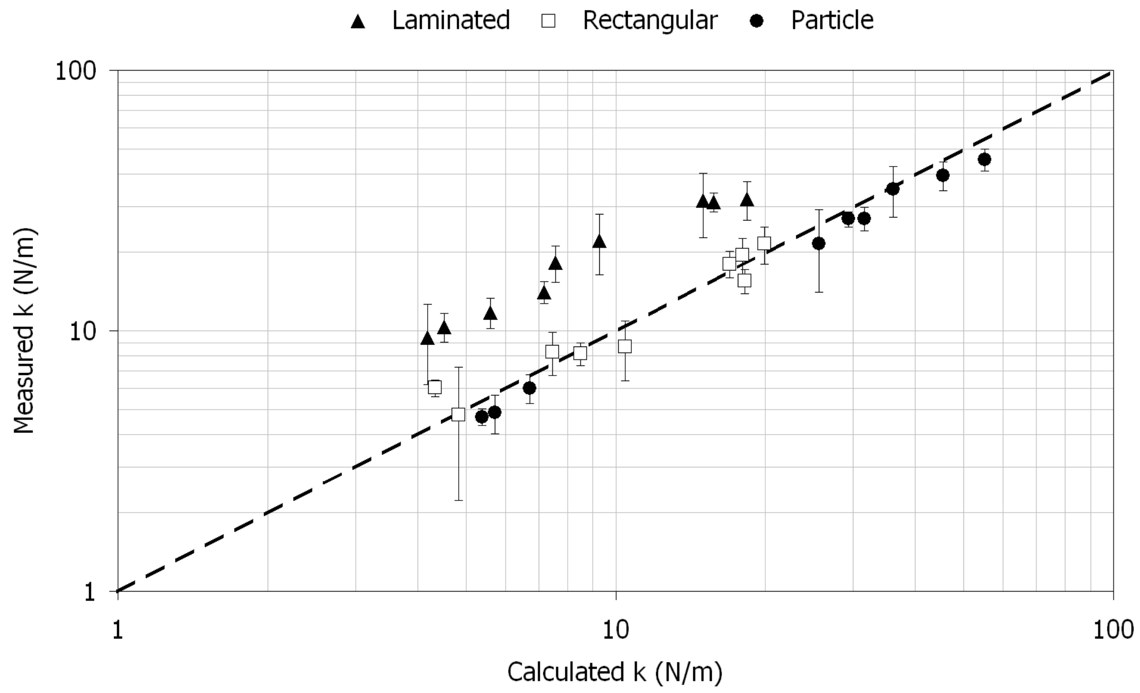

Figure 2. Percentage deviation between measured and calculated spring constants

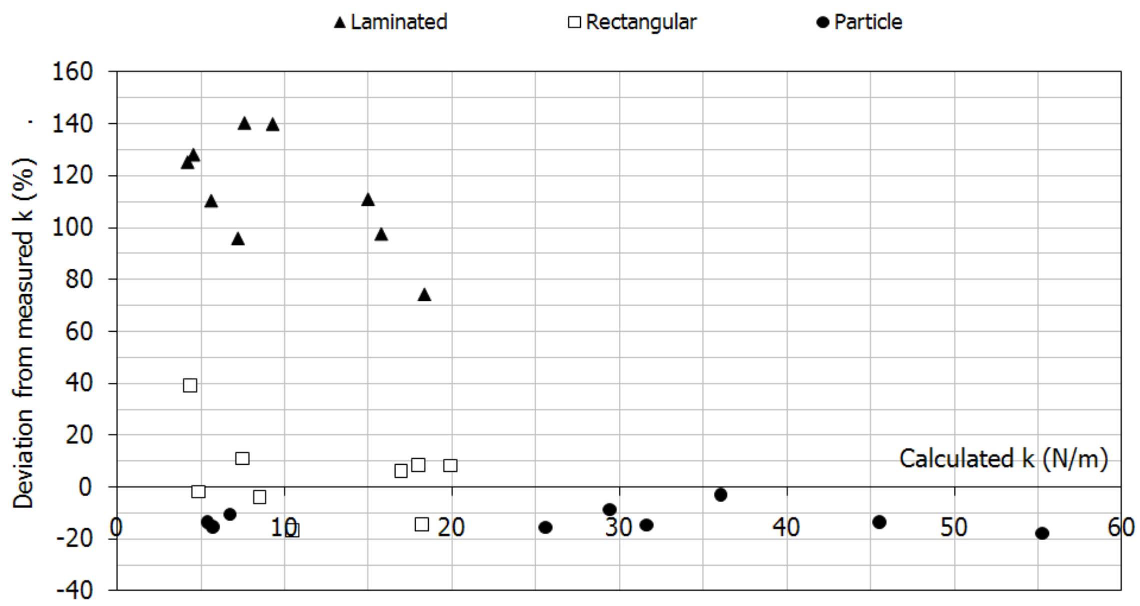

Figure 3. Measured spring constants as a function of cantilever resonant frequency

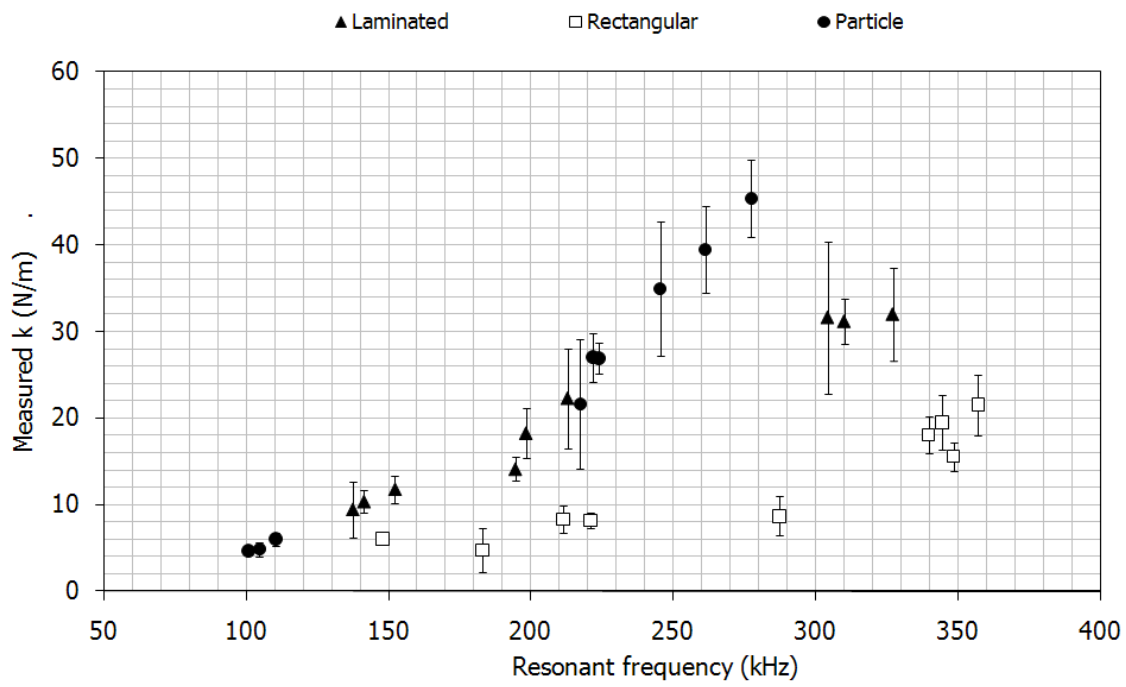

Tables

Table 1. Measured and calculated properties of rectangular cantilevers (35 μm width)

Cantilever label	Length (μm)	Measured spring constant (N/m)	Calculated spring constant (N/m)	Calculated Si thickness (μm)
R01	90	21.5 ± 3.5	19.9	2.2
R02	130	6.0 ± 0.5	4.3	2.0
R03	110	8.3 ± 1.6	7.5	2.0
R04	90	19.5 ± 3.2	18.0	2.2
R05	110	4.8 ± 2.5	4.8	1.7
R06	90	8.7 ± 2.3	10.4	1.8
R07	110	8.2 ± 0.8	8.5	2.1
R08	90	15.6 ± 1.7	18.2	2.2
R09	90	18.0 ± 2.1	17.0	2.1

Table 2. Measured and calculated properties of rectangular cantilevers modified with SiO_2 microparticles

Cantilever label	Length (µm)	Width (µm)	Measured spring constant (N/m)	Calculated spring constant (N/m)	Calculated Si thickness (µm)
P01	178	37	6.0 ± 0.7	6.7	2.9
P02	177	39	4.7 ± 0.3	5.4	2.6
P03	176	37	4.9 ± 0.8	5.8	2.7
P04	148	33	26.9 ± 1.8	29.4	4.0
P05	137	38	21.6 ± 7.5	25.6	3.4
P06	142	37	39.5 ± 5.0	45.5	4.3
P07	154	34	27.0 ± 2.8	31.1	4.3
P08	139	37	34.9 ± 7.7	36.1	3.9
P09	141	39	45.4 ± 4.4	55.2	4.5

Table 3. Measured and calculated properties of rectangular cantilevers laminated with 20 nm Cr and 20 nm Au thin films (35 μm width)

Cantilever label	Length (μm)	Calculated spring constant (N/m)	Calculated Si thickness (μm)	Calculated resonant frequency of the unloaded cantilever (Hz)	Calculated spring constant of the unloaded cantilever (N/m)
L01	110	7.58	1.8	220,709	10.3
L02	90	15.76	1.9	343,844	21.1
L03	130	4.19	1.8	153,387	5.7
L04	110	7.19	1.8	216,968	9.8
L05	90	14.97	1.9	338,027	20.1
L06	130	4.53	1.8	157,371	6.1
L07	110	9.27	2.0	235,467	12.3
L08	90	18.34	2.0	361,051	24.3
L09	130	5.59	2.0	168,392	7.4

Table 4. Change in resonant frequencies of rectangular Si cantilevers upon deposition of thin films of Cr or Ti

Cantilever label	Metal deposited	Unloaded resonant frequency (kHz)	Loaded resonant frequency (kHz)
CSC12-1A	Ti, 3 nm	124.674	124.812
CSC12-1B	Ti, 3 nm	200.839	200.946
CSC12-1C	Ti, 3 nm	87.568	87.604
CSC12-2A	Ti, 3 nm	135.146	135.151
CSC12-2B	Ti, 3 nm	213.257	213.061
CSC12-2C	Ti, 3 nm	92.696	92.545
CSC12-3A	Ti, 8 nm	133.923	134.382
CSC12-3B	Ti, 8 nm	213.257	201.957
CSC12-3C	Ti, 8 nm	92.696	92.466
CSC12-4A	Ti, 8 nm	132.380	133.073
CSC12-4B	Ti, 8 nm	196.672	197.879
CSC12-4C	Ti, 8 nm	91.188	91.890
CSC12-5A	Cr, 3 nm	136.284	136.431
CSC12-5B	Cr, 3 nm	205.554	205.699
CSC12-5C	Cr, 3 nm	93.886	93.995
CSC12-6A	Cr, 3 nm	150.686	150.832
CSC12-6B	Cr, 3 nm	207.851	207.769
CSC12-6C	Cr, 3 nm	94.396	94.482
CSC12-7A	Cr, 8 nm	129.236	129.564
CSC12-7B	Cr, 8 nm	187.414	187.729
CSC12-7C	Cr, 8 nm	88.221	88.543
CSC12-8A	Cr, 8 nm	130.538	131.061
CSC12-8B	Cr, 8 nm	201.565	201.301
CSC12-8C	Cr, 8 nm	93.829	94.129

Table 5. Percentage compositions of cantilever surfaces after deposition of thin films of Cr or Ti

Cantilever label	Metal deposited	Cr (%)	Ti (%)	Si (%)	O (%)
CSC12-1	Ti, 3 nm	-	4.38	7.11	88.51
CSC12-3	Ti, 8 nm	-	4.21	5.58	90.21
CSC12-5	Cr, 3 nm	6.75	-	8.04	85.21
CSC12-7	Cr, 8 nm	19.14	-	4.44	76.42

Table 6. Uncertainties associated with system parameters

System parameter	Value	Uncertainty	Effect on t (μm)	Effect on k (N/m)
Length (μm)	90	± 1	± 0.05	± 0.6
Width (μm)	35	± 1	± 0.01	± 0.5
Resonant frequency (Hz)	344,431	± 10	± 0.0001	± 0.002
Young's modulus (GPa)	152	± 1	± 0.005	± 0.005
Density (kg/m^3)	2,330	± 10	± 0.005	± 0.12

Table 7. Effect of uncertainty propagation

System parameter	Value	Lower bound	Upper bound
Length (μm)	90	89	91
Width (μm)	35	34	36
Resonant frequency (Hz)	344,431	344,421	344,441
Young's modulus (GPa)	152	151	153
Density (kg/m^3)	2,330	2,320	2,340
Thickness (μm)	2.13	2.08	2.17
Spring constant (N/m)	17.54	16.43	18.71

Appendix: Calculation of the flexural rigidity of an asymmetrically laminated beam

In order to calculate the flexural rigidity of an asymmetrically laminated beam, the composite beam method was used. In essence, this method states that at the neutral axis (see Figure A1), bending stresses are zero and all forces are in equilibrium, i.e.:

$$\sum F_x = 0 = \int_A \sigma_b dA = \int_{A,Si} \sigma_{b,Si} dA_{Si} + \int_{A,Cr} \sigma_{b,Cr} dA_{Cr} + \int_{A,Au} \sigma_{b,Au} dA_{Au}$$

where σ_b is the stress in each layer and A is the cross-sectional area.

Figure A1. Schematic of cross-section of beam

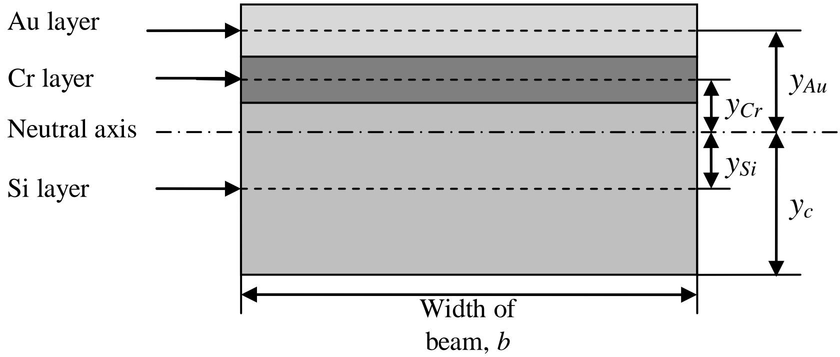

For pure bending, the stresses can be given as $\sigma_b = \frac{-Ey}{\rho}$, where ρ is the radius of curvature, y is the distance to the neutral axis and E is the Young's modulus of the layer and therefore:

$$0 = \int_{A,Si} \frac{-E_{Si} y_{Si}}{\rho} dA_{Si} + \int_{A,Cr} \frac{-E_{Cr} y_{Cr}}{\rho} dA_{Cr} + \int_{A,Au} \frac{-E_{Au} y_{Au}}{\rho} dA_{Au}$$

$$= E_{Si} \int_{A,Si} \frac{y_{Si}}{\rho} dA_{Si} + E_{Cr} \int_{A,Cr} \frac{y_{Cr}}{\rho} dA_{Cr} + E_{Au} \int_{A,Au} \frac{y_{Au}}{\rho} dA_{Au}$$

$$= E_{Si} y_{Si} A_{Si} + E_{Cr} y_{Cr} A_{Cr} + E_{Au} y_{Au} A_{Au}$$

$$= E_{Si} \left(\frac{t_{Si}}{2} - y_c \right) bt_{Si} + E_{Cr} \left(t_{Si} + \frac{t_{Cr}}{2} - y_c \right) bt_{Cr} + E_{Au} \left(t_{Si} + t_{Cr} + \frac{t_{Au}}{2} - y_c \right) bt_{Au}$$

$$= E_{Si} y_c bt_{Si} + \frac{E_{Si}}{2} bt_{Si}^2 + E_{Cr} bt_{Si} t_{Cr} + \frac{E_{Cr}}{2} bt_{Cr}^2 - E_{Cr} y_c bt_{Cr} + E_{Au} bt_{Si} t_{Au} + E_{Au} bt_{Cr} t_{Au} + \frac{E_{Au}}{2} bt_{Au}^2 - E_{Au} y_c bt_{Au}$$

Collecting terms gives:

$$\left(E_{Si} t_{Si} + E_{Cr} t_{Cr} + E_{Au} t_{Au} \right) y_c = \frac{E_{Si}}{2} t_{Si}^2 + E_{Cr} t_{Cr} \left(t_{Si} + \frac{t_{Cr}}{2} \right) + E_{Au} t_{Au} \left(t_{Si} + t_{Cr} + \frac{t_{Au}}{2} \right)$$

Hence the location of the neutral axis can be given by:

$$y_c = \frac{E_{Si} t_{Si}^2 + E_{Cr} t_{Cr} \left(2t_{Si} + t_{Cr} \right) + E_{Au} t_{Au} \left(2t_{Si} + 2t_{Cr} + t_{Au} \right)}{2 \left(E_{Si} t_{Si} + E_{Cr} t_{Cr} + E_{Au} t_{Au} \right)}$$

Using the parallel axis theorem, $I = I_{cm} + Ay^2$, we obtain:

$$I_{Si} = \frac{bt_{Si}^3}{12} + bt_{Si}\left(\frac{t_{Si}}{2} - y_c\right)^2 = \frac{b}{3}\left[(t_{Si} - y_c)^3 + y_c^3\right]$$

$$I_{Cr} = \frac{bt_{Cr}^3}{12} + bt_{Cr}\left(t_{Si} + \frac{t_{Cr}}{2} - y_c\right)^2 = \frac{b}{3}\left[(t_{Si} + t_{Cr} - y_c)^3 - (t_{Si} - y_c)^3\right]$$

$$I_{Au} = \frac{bt_{Au}^3}{12} + bt_{Au}\left(t_{Si} + t_{Cr} + \frac{t_{Au}}{2} - y_c\right)^2$$

And therefore the flexural rigidity of the entire beam can be given as:

$$EI = E_{Si}I_{Si} + E_{Cr}I_{Cr} + E_{Au}I_{Au}$$